

A Framework for Generating Semantically Ambiguous Images to Probe Human and Machine Perception

Yuqi Hu¹ Vasha DuTell^{1,2} Ahna R. Girshick¹ Jennifer E. Corbett²

¹University of California, Berkeley ²Massachusetts Institute of Technology

{yuqihu, ahna, vasha}@berkeley.edu {vasha, j8675309}@mit.edu

Abstract

The classic duck-rabbit illusion reveals that when visual evidence is ambiguous, the human brain must decide what it sees. But where exactly do human observers draw the line between “duck” and “rabbit”, and do machine classifiers draw it in the same place? We use semantically ambiguous images as interpretability probes to expose how vision models represent the boundaries between concepts. We present a psychophysically-informed framework that interpolates between concepts in the CLIP embedding space to generate continuous spectra of ambiguous images, allowing us to precisely measure where and how humans and machine classifiers place their semantic boundaries. Using this framework, we show that machine classifiers are more biased towards seeing “rabbit”, whereas humans are more aligned with the CLIP embedding used for synthesis, and the guidance scale seems to affect human sensitivity more strongly than machine classifiers. Our framework demonstrates how controlled ambiguity can serve as a diagnostic tool to bridge the gap between human psychophysical analysis, image classification, and generative image models, offering insight into human-model alignment, robustness, model interpretability, and image synthesis methods.

1. Introduction and Previous Work

The classic duck-rabbit illusion shown in Fig. 1 (left) illustrates a striking property of perception: a single image can support multiple valid interpretations. Observers may perceive either a duck or a rabbit, revealing how the visual system resolves competing hypotheses when sensory evidence is ambiguous. Psychophysics [32], a quantitative methodology for probing human perception, relies on a controlled continuum of stimuli. Classic bistable stimuli based on low-level visual cues, such as the Necker cube and Rubin’s vase, have long served as probes of perceptual ambiguity [24]. In contrast, the duck-rabbit is ambiguous at the semantic meaning level — a form of indeterminate im-

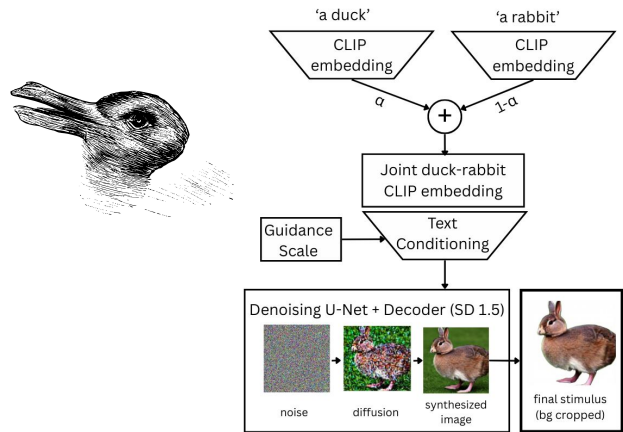


Figure 1. **Left:** The classic duck-rabbit illusion [19] is a well-known example of perceptual ambiguity, where the same image can be seen as either a duck or a rabbit. **Right:** Our process for generating ambiguous stimuli.

agery [14, 28] that is difficult to parameterize for systematic psychophysical measurement.

Text-to-image diffusion models offer a new way to generate such diagnostic stimuli cheaply and quickly. Latent diffusion models [35] enable efficient, high-fidelity image synthesis conditioned on text embeddings. Rather than relying on hand-crafted figures for ambiguous semantic meaning, we can now generate continuous spectra of stimuli that transition smoothly from one semantic concept to another, and directly connect that continuum to a perceptual metric.

From a machine learning perspective, this comparison matters for understanding the geometry of learned visual representations. Recent machine vision systems, from CLIP [31] to ImageNet classifiers [36], learn to organize images into semantic labels, but the structure of these learned semantic spaces remains difficult to interpret when training data lacks indeterminate images and labels, including indeterminate objects such as a duck-rabbit. Furthermore, applying psychophysical measures to compare hu-

man and machine semantic perception requires a reconciliation of their response formats (e.g., 2AFC vs. one-hot).

Here, we combine controlled generative semantic ambiguity with human psychophysics and machine classifier evaluation in a novel approach to compare how humans and models resolve semantic competition. By interpolating between text embeddings, mixing “a duck” with “a rabbit” in varying proportions, we can produce stimuli that range from unambiguously duck-like, through maximally ambiguous duck-rabbit hybrids, to unambiguously rabbit-like. Furthermore, by leveraging classifier-free guidance [15], the strength of adherence to these conditioning prompts can be controlled by varying the classifier-free guidance scale (GS). We then measure semantic judgments from human observers using a two-alternative forced choice (2AFC) task, and from pretrained ImageNet classifiers by aggregating softmax probabilities over relevant semantic categories, inferring a model’s “choice”. This stimulus continuum along semantic mixing ratio (α) levels can be fit by a psychometric function for both humans and models, at each guidance scale, to estimate perceptual bias and sensitivity. This approach treats diffusion models not merely as image generators but as tools for probing the structure of visual semantic spaces. By understanding and comparing the semantic boundaries of human and machine systems, we can better understand their internal representations, with applications in robustness, human-alignment, model interpretability, image synthesis, and a bridge from machine learning to perceptual science.

2. A Framework for Semantic Ambiguity

We present a framework with three components: (1) stimulus images generated along a continuum of semantic ambiguity, (2) perceptual measurements along the same continuum using psychophysical methodology, and (3) bias and sensitivity outputs allowing comparisons within and between human and machine observers.

2.1. Stimulus Generation Along a Continuum

In Fig. 1 (right), we show our process for generating the stimuli, using Stable Diffusion v1.5 [39] with the standard latent diffusion model formulation using DDPM noise-prediction loss [16], and CLIP text encoder conditioning [31], combined with classifier-free guidance [15]. To obtain a smooth semantic-morph continuum, we linearly interpolate CLIP embeddings using a mixing-ratio parameter (α) with $\alpha \in [0, 1]$ defined in CLIP embedding space. For the rabbit-duck experiment (see Supplement for an elephant-rabbit experiment), two base prompts (“a duck” and “a rabbit”) were encoded into text embedding vectors emb_{duck} and $\text{emb}_{\text{rabbit}}$, and the conditional embedding used

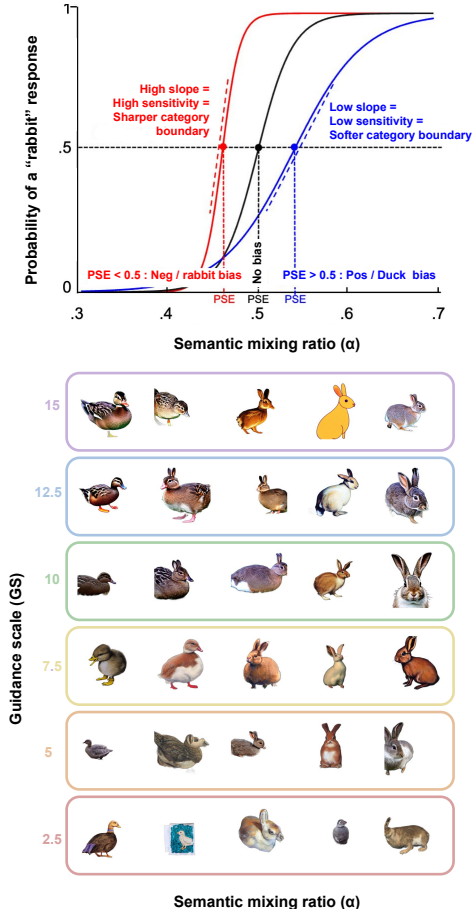


Figure 2. **Top:** Illustrative psychometric function and effects on bias and sensitivity as a function of semantic mixing ratio (α). **Bottom:** Example stimuli as a function of semantic mixing ratio (α) and guidance scale (GS).

for generation was:

$$\text{lerp_cond}(\alpha) = (1 - \alpha) \text{emb}_{\text{duck}} + \alpha \text{emb}_{\text{rabbit}}. \quad (1)$$

Setting $\alpha = 0$ produces a duck-dominant image; $\alpha = 1$ produces a rabbit-dominant image; and in between values yield hybrid duck-rabbit images. We factorially combined six guidance scales $\{2.5, 5.0, 7.5, 10.0, 12.5, 15.0\}$ with five α levels $\{0.3, 0.4, 0.5, 0.6, 0.7\}$, selected after piloting to span the full psychometric range without unnecessary asymptotic levels. Ten synthesis seeds per condition produced 300 images (60 denoising steps each) (Fig. 2 (bottom) and Supplemental for the full stimulus set (Sec. 5.1)).

2.2. Psychophysics on a Matched Continuum

Humans. We measured human participant responses to these images in a 2AFC experiment (Supplemental). For each participant and guidance scale, we computed the proportion of “rabbit” responses at each of the five α levels and

Observer		Observer								
		Human	ConvNeXt-Base	DenseNet-121	EfficientNet-B0	MobileNetV3-L	ResNet-50	ViT-B/16	AlexNet	CORnet-S
GS										
2.5	0.00	-0.14	-0.09	-0.08	-0.12	-0.10	-0.11	-0.13	-0.11	
5.0	-0.02	-0.09	-0.07	-0.12	-0.11	-0.09	-0.07	-0.09	-0.11	
7.5	-0.02	-0.08	-0.06	-0.09	-0.10	-0.08	-0.05	-0.07	-0.08	
10.0	-0.03	-0.07	-0.08	-0.10	-0.08	-0.07	-0.08	-0.04	-0.09	
12.5	-0.01	-0.04	-0.07	-0.07	-0.06	-0.06	-0.08	-0.02	-0.10	
15.0	-0.01	-0.06	-0.06	-0.07	-0.06	-0.07	-0.05	0.00	-0.06	

Table 1. **Bias for humans and classifier models.** White denotes zero bias. Red denotes negative bias (toward rabbits), and blue denotes positive bias (toward ducks). Color intensity is computed using global min–max normalization across all entries. All entries are non-positive, indicating a consistent bias toward rabbits across observers.

Observer		Observer								
		Human	ConvNeXt-Base	DenseNet-121	EfficientNet-B0	MobileNetV3-L	ResNet-50	ViT-B/16	AlexNet	CORnet-S
GS										
2.5	3.94	6.68	7.17	7.14	7.59	6.73	6.22	5.70	6.21	
5.0	6.20	7.61	6.73	7.14	7.61	7.17	7.61	6.72	7.61	
7.5	6.37	7.15	7.17	7.17	7.61	6.73	7.62	7.17	7.61	
10.0	6.35	7.62	7.61	7.61	7.61	7.61	7.61	6.66	7.14	
12.5	6.08	6.70	7.62	7.10	7.61	7.17	7.15	6.20	6.68	
15.0	6.79	7.62	7.62	7.62	7.62	7.62	7.62	6.63	7.15	

Table 2. **Sensitivity for humans and classifier models.** Darker red indicates higher sensitivity (steeper psychometric slope).

fit a logistic psychometric function with equal upper and lower asymptotes using the psignifit 4 toolbox [37]:

$$P(\text{rabbit}) = \frac{1}{1 + \exp[-\beta_1(\alpha - \text{PSE})]}. \quad (2)$$

We extracted two summary parameters, β_1 and PSE, per fitted curve and used them to calculate bias and sensitivity. The point of subjective equality (PSE) corresponds to the α threshold at which one is equally likely to say rabbit or duck ($P(\text{rabbit}) = 0.5$) (Fig. 2 (top)). A PSE of 0.5 represents an unbiased observer who is equally likely to choose rabbit or duck at $\alpha = 0.5$. We define:

$$\text{Bias} = \text{PSE} - 0.5, \quad \text{Sensitivity} = \beta_1 \quad (3)$$

where β_1 is the slope of the psychometric function at the PSE. The slope determines how sharply responses transition between semantic meaning as α varies around the decision boundary. Grand-average parameters were obtained by averaging the individual estimates of bias and sensitivity across participants, and standard errors of the mean were computed for each parameter (Fig. 5, Supplemental).

Machine Classifiers. We evaluated the same 300 images using eight pretrained ImageNet classifiers (Table 4, Supplemental). To make the machine evaluation structurally parallel to the human 2AFC design, we treated each of the 10 seeds (synthesized images) as an independent trial. For each image, we extracted softmax probabilities over all ImageNet classes and computed the probability of a rabbit response as:

$$P(\text{rabbit}) = \frac{\bar{p}_{\text{rabbit}}}{\bar{p}_{\text{rabbit}} + \bar{p}_{\text{duck}}}, \quad \bar{p}_a = \frac{1}{|\mathcal{A}_L|} \sum_{i \in \mathcal{A}_L} p_i, \quad (4)$$

where L denotes an ImageNet-1K label, \mathcal{A}_L is the set of ImageNet labels for a particular animal, p_i denotes the softmax probability assigned to each ImageNet-1K label in \mathcal{A}_L , \bar{p}_a denotes the average softmax probability over all relevant labels for each animal class, normalized by the number of labels for that animal $|\mathcal{A}_L|$ (Table 5, Supplemental).

Each binary response was then sampled from a Bernoulli distribution with this probability. The proportion of rabbit responses across the 10 images served as the machine analog of the human proportion-rabbit measure, and psychometric functions were fit using the same procedure as for human data. In addition to the duck-rabbit experiment, we also conducted an elephant-rabbit experiment, evaluating a set of human participants and the same models, interpolating between the CLIP embeddings corresponding to “an elephant” and “a rabbit”.

2.3. Framework Output & Interpretation

Validation of Framework. We find our generative image system with matched psychophysical pipeline performed as intended across both human observers and machine classifiers. The α interpolation parameter produced well-behaved perceptual continua: both human and machine response proportions transitioned smoothly and largely monotonically from duck to rabbit across the five α levels, confirming that linear interpolation in CLIP embedding space generates stimuli that are treated as a coherent semantic continuum by both biological and artificial vision systems. The psychometric functions themselves showed good coverage of the full response range (Fig. 5, Supplemental) and their goodness-of-fit scores are within acceptable ranges (Table 3, Supplemental).

Bias. Across the guidance scales, for the duck-rabbit condition, the grand-average human biases ranged from

0.00 to -0.03, with an average of -0.015 (on a scale of -0.5 to 0.5), indicating that human participants were only slightly biased towards rabbit, placing the duck-rabbit boundary near the midpoint of the CLIP-defined semantic mixing continuum (α) (Table 1, Fig. 6 and Fig. 7, Supplemental). By contrast, the classifier models tested showed much more rabbit bias. This differential bias between humans and classifiers was consistent across architectures. One exception is AlexNet, which showed high bias at low guidance scales, but more human-like low bias at higher guidance scales. There may be an effect of bias decreasing with increasing guidance scale for classifiers, which warrants further testing. In evaluating the elephant-rabbit condition (Table 6, Fig. 10 and Fig. 11, Supplemental), we find qualitatively similar decreased bias in humans as compared to classifiers; however, classifiers are less biased than in the duck-rabbit condition, and the effect of guidance scale is less visible. In the elephant-rabbit condition, AlexNet is again an outlier, in this case showing a bias towards elephants as compared to the other models.

Sensitivity. For the duck-rabbit condition, between guidance scales 2.5 and 5, the grand-average human sensitivity jumps from 3.94 to a plateau at around 6.25 (Table 2, Fig. 6 and Fig. 8, Supplemental). By comparison, classifier models show higher sensitivity overall, indicating sharper semantic boundaries, and a few of the classifier models also may show this increase between GS = 2.5 and 5.

In evaluating the elephant-rabbit condition (Table 7, Fig. 10 and Fig. 12, Supplemental), we find mostly similar increased sensitivity in the classifiers as compared to humans, with the exception being the pronounced human peak sensitivity around GS = 10. As in the duck-rabbit condition, some of the classifiers also display a jump in sensitivity between GS = 2.5 and 5.

3. Discussion and Future Directions

Semantically ambiguous images such as the duck-rabbit illusion have long served as compelling demonstrations of perceptual ambiguity [19, 34], but have been difficult to deploy in psychophysical experiments due to the need for controlled stimulus continua [32]. Our framework provides a simple and scalable method for generating images along a continuum of semantic ambiguity, enabling systematic measurement of perceptual decision boundaries. The same paradigm can be applied to both human observers and machine vision models, enabling direct comparison of bias and sensitivity across humans, across models, and between humans and models.

Across two conditions, we find that human observers exhibit less semantic bias than classifier models, placing decision boundaries closer to the midpoint of the CLIP interpolation [31]. This suggests that human perception may be more aligned with the semantic structure captured by CLIP

embeddings, whereas classifiers trained for discrete categorization may develop sharper or shifted decision boundaries. This divergence highlights a limitation of standard classification training objectives, which do not explicitly constrain behavior near semantic meaning boundaries. Our results therefore provide empirical support for classifier-free guidance [15] in image synthesis: classifier-based guidance can shift perceived content away from the intended concept. An open question is whether these biases originate primarily from the training data and objectives of the classifiers, or from the statistics of the generated images themselves, which may already encode asymmetries in pixel space. Disentangling these factors will be important for understanding and mitigating bias in generative pipelines. Extending this framework to a wider range of label pairs, such as all pairs of ImageNet animals [36], could provide a more comprehensive map of semantic organization in both human and machine vision.

We further observe that classifier models tend to exhibit higher sensitivity than humans, potentially reflecting differences in internal noise, decision strategies, or the absence of lapse-like behavior in deterministic models [29]. In some cases, both bias and sensitivity vary with guidance scale, suggesting that guidance modulates not only image quality but also the structure of ambiguity in generated stimuli. This raises the possibility of an optimal guidance regime for controlling perceptual ambiguity, depending on stimulus class and model architecture. More generally, this suggests that guidance scale may act as a control over the sharpness of semantic transitions in generated images, rather than only a fidelity parameter.

Interestingly, different classifier architectures show broadly similar behavior despite substantial differences in design. Vision transformers [5] and convolutional networks [13] yield comparable perceptual boundaries, and even architectures motivated by biological vision, such as CORnet [23], do not exhibit substantially more human-like behavior. AlexNet [22] shows occasional deviations, possibly reflecting its simpler architecture. These results suggest perceptual boundaries may be shaped by factors other than architecture, such as training objectives and datasets. Future work should extend this analysis to a broader range of models, including self-supervised systems such as DINO [27].

More broadly, our results point to differences in the internal geometry of visual representations. Human and machine systems appear to organize semantic meaning differently, leading to systematic shifts in decision boundaries. Our results show that perceptual decision boundaries do not necessarily align with the midpoint of CLIP interpolations, suggesting that distances in embedding space are not directly predictive of human perceptual similarity [6, 7]. A promising direction for future work is to characterize how embedding geometry relates to perceptual transitions across

the semantic image manifold, and to use psychophysical measurements to refine these representations toward better human alignment. Our framework demonstrates how controlled semantic ambiguity can be used to probe and align visual representations, bridging human perception, discriminative models, and generative systems.

References

- [1] Tal Boger and Chaz Firestone. Visual anagrams reveal high-level effects with ‘identical’ stimuli. *Current Biology*, 35(19):R910–R912, 2025. 7
- [2] Andrew Brock, Jeff Donahue, and Karen Simonyan. Large scale gan training for high fidelity natural image synthesis. *arXiv preprint arXiv:1809.11096*, 2018. 7
- [3] Ryan Burgert, Xiang Li, Abe Leite, Kanchana Ranasinghe, and Michael Ryoo. Diffusion illusions: Hiding images in plain sight. In *ACM SIGGRAPH 2024 Conference Papers*, pages 1–11, 2024. 7
- [4] Arturo Deza and Talia Konkle. Emergent properties of foveated perceptual systems. *arXiv preprint arXiv:2006.07991*, 2020. 7
- [5] Alexey Dosovitskiy, Lucas Beyer, Alexander Kolesnikov, Dirk Weissenborn, Xiaohua Zhai, Thomas Unterthiner, Mostafa Dehghani, Matthias Minderer, Georg Heigold, Sylvain Gelly, et al. An image is worth 16x16 words: Transformers for image recognition at scale. *arXiv preprint arXiv:2010.11929*, 2020. 4, 8, 10
- [6] Jenelle Feather, Alex Durango, Ray Gonzalez, and Josh McDermott. Metamers of neural networks reveal divergence from human perceptual systems. In *Advances in Neural Information Processing Systems*, pages 10078–10089, 2019. 4, 7
- [7] Jeremy Freeman and Eero P Simoncelli. Metamers of the ventral stream. *Nature neuroscience*, 14(9):1195–1201, 2011. 4, 7
- [8] Leon A Gatys, Alexander S Ecker, and Matthias Bethge. Image style transfer using convolutional neural networks. In *Proceedings of the IEEE conference on computer vision and pattern recognition*, pages 2414–2423, 2016. 7
- [9] Robert Geirhos, Patricia Rubisch, Claudio Michaelis, Matthias Bethge, Felix A Wichmann, and Wieland Brendel. Imagenet-trained cnns are biased towards texture; increasing shape bias improves accuracy and robustness. In *International conference on learning representations*, 2018. 7
- [10] Daniel Geng, Inbum Park, and Andrew Owens. Visual anagrams: Generating multi-view optical illusions with diffusion models. In *Proceedings of the IEEE/CVF Conference on Computer Vision and Pattern Recognition*, pages 24154–24163, 2024. 7
- [11] Arnulf BA Graf, Felix A Wichmann, Heinrich H Bülthoff, and Bernhard Schölkopf. Classification of faces in man and machine. *Neural Computation*, 18(1):143–165, 2006. 7
- [12] Anne Harrington, Vasha DuTell, Mark Hamilton, Ayush Tewari, Simon Stent, William T Freeman, and Ruth Rosenholtz. Coco-periph: bridging the gap between human and machine perception in the periphery. In *The Twelfth International Conference on Learning Representations*, 2023. 7
- [13] Kaiming He, Xiangyu Zhang, Shaoqing Ren, and Jian Sun. Deep residual learning for image recognition. In *Proceedings of the IEEE conference on computer vision and pattern recognition*, pages 770–778, 2016. 4, 8, 10
- [14] Aaron Hertzmann. Visual indeterminacy in gan art. In *ACM SIGGRAPH 2020 Art Gallery*, page 424–428, New York, NY, USA, 2020. Association for Computing Machinery. 1, 7
- [15] Jonathan Ho and Tim Salimans. Classifier-free diffusion guidance. *arXiv preprint arXiv:2207.12598*, 2022. 2, 4
- [16] Jonathan Ho, Ajay Jain, and Pieter Abbeel. Denoising diffusion probabilistic models. *Advances in neural information processing systems*, 33:6840–6851, 2020. 2
- [17] Andrew Howard, Mark Sandler, Grace Chu, Liang-Chieh Chen, Bo Chen, Mingxing Tan, Weijun Wang, Yukun Zhu, Ruoming Pang, Vijay Vasudevan, et al. Searching for mobilenetv3. In *Proceedings of the IEEE/CVF international conference on computer vision*, pages 1314–1324, 2019. 8, 10
- [18] Gao Huang, Zhuang Liu, Laurens Van Der Maaten, and Kilian Q Weinberger. Densely connected convolutional networks. In *Proceedings of the IEEE conference on computer vision and pattern recognition*, pages 4700–4708, 2017. 8, 10
- [19] Joseph Jastrow. Duck-rabbit illusion. *The mind’s eye. Popular Science Monthly*, 54:299–312, 1899. 1, 4
- [20] Tero Karras, Samuli Laine, and Timo Aila. A style-based generator architecture for generative adversarial networks. In *Proceedings of the IEEE/CVF conference on computer vision and pattern recognition*, pages 4401–4410, 2019. 7
- [21] David C Knill and Alexandre Pouget. The bayesian brain: the role of uncertainty in neural coding and computation. *TRENDS in Neurosciences*, 27(12):712–719, 2004. 7
- [22] Alex Krizhevsky, Ilya Sutskever, and Geoffrey E Hinton. Imagenet classification with deep convolutional neural networks. *Advances in neural information processing systems*, 25, 2012. 4, 8, 10
- [23] Jonas Kubilius, Martin Schrimpf, Kohitij Kar, Rishi Rajalingham, Ha Hong, Najib Majaj, Elias Issa, Pouya Bashivan, Jonathan Prescott-Roy, Kailyn Schmidt, et al. Brain-like object recognition with high-performing shallow recurrent nets. *Advances in neural information processing systems*, 32, 2019. 4, 8, 10
- [24] David A. Leopold and Nikos K. Logothetis. Multistable phenomena: changing views in perception. *Trends in Cognitive Sciences*, 3(7):254–264, 1999. 1, 7
- [25] Zhuang Liu, Hanzi Mao, Chao-Yuan Wu, Christoph Feichtenhofer, Trevor Darrell, and Saining Xie. A convnet for the 2020s. In *Proceedings of the IEEE/CVF conference on computer vision and pattern recognition*, pages 11976–11986, 2022. 8, 10
- [26] Anh Nguyen, Jason Yosinski, and Jeff Clune. Deep neural networks are easily fooled: High confidence predictions for unrecognizable images. In *Computer Vision and Pattern Recognition (CVPR), 2015 IEEE Conference on*. IEEE, 2015. 7
- [27] Maxime Oquab, Timothée Darcet, Théo Moutakanni, Huy Vo, Marc Szafraniec, Vasil Khalidov, Pierre Fernandez,

- Daniel Haziza, Francisco Massa, Alaaeldin El-Nouby, et al. Dinov2: Learning robust visual features without supervision. *arXiv preprint arXiv:2304.07193*, 2023. 4
- [28] Robert Pepperell. Seeing without objects: Visual indeterminacy and art. *Leonardo*, 39(5):394–400, 2006. 1, 7
- [29] Joshua C Peterson, Ruairidh M Battleday, Thomas L Griffiths, and Olga Russakovsky. Human uncertainty makes classification more robust. In *Proceedings of the IEEE/CVF international conference on computer vision*, pages 9617–9626, 2019. 4, 8
- [30] Ben Poole, Ajay Jain, Jonathan T Barron, and Ben Mildenhall. Dreamfusion: Text-to-3d using 2d diffusion. *arXiv preprint arXiv:2209.14988*, 2022. 7
- [31] Alec Radford, Jong Wook Kim, Chris Hallacy, Aditya Ramesh, Gabriel Goh, Sandhini Agarwal, Girish Sastry, Amanda Askell, Pamela Mishkin, Jack Clark, et al. Learning transferable visual models from natural language supervision. In *International conference on machine learning*, pages 8748–8763. PmLR, 2021. 1, 2, 4
- [32] Jenny C. A. Read. The place of human psychophysics in modern neuroscience. *Neuroscience*, 296:116–129, 2015. 1, 4
- [33] Eitan Richardson and Yair Weiss. A bayes-optimal view on adversarial examples. *Journal of Machine Learning Research*, 22(221):1–28, 2021. 7
- [34] Irvin Rock. *The Logic of Perception*. MIT Press, Cambridge, MA, 1983. 4, 7
- [35] Robin Rombach, Andreas Blattmann, Dominik Lorenz, Patrick Esser, and Björn Ommer. High-resolution image synthesis with latent diffusion models. In *Proceedings of the IEEE/CVF conference on computer vision and pattern recognition*, pages 10684–10695, 2022. 1, 7
- [36] Olga Russakovsky, Jia Deng, Hao Su, Jonathan Krause, Sanjeev Satheesh, Sean Ma, Zhiheng Huang, Andrej Karpathy, Aditya Khosla, Michael Bernstein, et al. Imagenet large scale visual recognition challenge. *International journal of computer vision*, 115(3):211–252, 2015. 1, 4, 8
- [37] Heiko H Schütt, Stefan Harmeling, Jakob H Macke, and Felix A Wichmann. Painfree and accurate bayesian estimation of psychometric functions for (potentially) overdispersed data. *Vision research*, 122:105–123, 2016. 3
- [38] Joel Simon. Artbreeder. <https://www.artbreeder.com>, 2018. Accessed: 2026. 7
- [39] stable-diffusion v1.5. <https://huggingface.co/stable-diffusion-v1-5/stable-diffusion-v1-5>, 2024. 2
- [40] Christian Szegedy, Wojciech Zaremba, Ilya Sutskever, Joan Bruna, Dumitru Erhan, Ian Goodfellow, and Rob Fergus. Intriguing properties of neural networks. *arXiv preprint arXiv:1312.6199*, 2013. 7
- [41] Mingxing Tan and Quoc Le. Efficientnet: Rethinking model scaling for convolutional neural networks. In *International conference on machine learning*, pages 6105–6114. PMLR, 2019. 8, 10
- [42] Matthew Tancik. Illusion diffusion: optical illusions using stable diffusion, 2023. 7
- [43] Felix A Wichmann and N Jeremy Hill. The psychometric function: I. fitting, sampling, and goodness of fit. *Perception & psychophysics*, 63(8):1293–1313, 2001. 8
- [44] Zhenglong Zhou and Chaz Firestone. Humans can decipher adversarial images. *Nature communications*, 10(1):1334, 2019. 8

A Framework for Generating Semantically Ambiguous Images to Probe Human and Machine Perception

Supplementary Material

In the Supplemental, we include the following materials:

- An expanded related work discussion (Supplemental 4).
- Details on our framework and its outputs (Supplemental 5).
- The elephant-rabbit condition (Supplemental 6).

4. Related Work

Ambiguity in Human Perception. Ambiguity is a fundamental property of human perception, reflecting sensory input that is noisy and compatible with multiple interpretations. The human visual system unconsciously performs probabilistic inference, integrating multiple pieces of sensory evidence with prior knowledge to attempt to resolve the uncertainty [21]. We become aware of this inference when viewing a bistable or indeterminate image. *Bistable images* yield two discrete interpretations that may alternate spontaneously despite a constant stimulus, such as in the classic duck-rabbit illusion [24, 34]. Bistable images have been extensively studied using psychophysical methods that quantify dominance durations, switching dynamics, and perceptual bias [24]. In contrast, *indeterminate imagery* lacks sufficient perceptual evidence to support a coherent interpretation, resisting categorization and foregrounding perceptual limits [14, 28]. While widely discussed in perceptual theory and art practice, indeterminate images have been less systematically studied with controlled psychophysics.

Generative Ambiguous Imagery. Early work on neural style transfer demonstrated that deep generative models can blend visual structures and stylistic features from multiple images, producing hybrid imagery that combines characteristics of different sources [8]. Such methods highlighted how learned visual representations can interpolate between visual semantic concepts and generate perceptually mixed images. Related interactive systems such as Artbreeder [38] leverage generative adversarial networks, including StyleGAN [20] and BigGAN [2], to allow users to explore and blend images in latent space. These approaches show that generative models can interpolate visual semantics, but they do not control ambiguity along a perceptual continuum.

More recent work has used generative models to construct images that support multiple interpretations while keeping low-level image statistics largely consistent [1]. Diffusion Illusion [3] adopts an explicit optimization-based method using score distillation sampling (SDS) [30] to align different prompts with different views. While effective, the reliance on SDS leads to long sampling times and often

lower visual quality. In contrast, Visual Anagrams [10] proposes a step-by-step multi-view denoising procedure that enforces prompt consistency across views during sampling. Illusion Diffusion [42], which generates rotation-based illusions by sampling from a latent diffusion model [35], is closer to a compact implementation of multi-view prompt consistency without explicit optimization. These generative illusion methods primarily generate multi-view illusions, where different geometric transformations reveal different semantic interpretations. In contrast, we introduce a framework for generating continuous semantic ambiguities within a single view, enabling psychophysical measurement of perceptual decision boundaries.

Comparison of Human and Machine Perception of Generative Imagery.

A growing body of work compares human perception with the behavior of modern vision models, revealing both shared sensitivities and systematic divergences. Early studies showed that deep convolutional networks trained for object recognition can achieve high performance on benchmark datasets while relying on image features that differ substantially from those used by humans [9]. Subsequent work has explored these differences using controlled visual stimuli, including adversarial perturbations [40], metamers generated from model representations [6, 7, 12], and images optimized to strongly activate individual neurons or classes [26]. These approaches show that models can make confident predictions on images that humans find ambiguous or misleading.

Beyond individual stimuli, another line of work compares the categorical decision boundaries of humans and machines, often motivated by improving robustness and human alignment. Human and machine decision boundaries can be directly compared using psychophysical methods, with boundary-based classifiers such as SVMs better capturing human internal decision space than prototype-based approaches [11]. CNN training consistently learns suboptimal decision boundaries, with SVMs learning boundaries closer to optimal on identical training data [33]. ImageNet-trained CNNs also exhibit a strong texture bias in stark contrast to humans, revealing fundamentally different classification strategies even when accuracy is matched [9]. Related work shows that modifying architectural assumptions such as introducing biologically inspired foveated representations can substantially alter the representational properties and robustness of vision models [4]. In addition, adversarial images that fool neural networks can sometimes transfer to

human observers under brief presentation or controlled conditions [44]. Other studies have constructed image continua between categories to measure decision boundaries in humans and models [29]. However, generating controlled ambiguous stimuli remains challenging, particularly when the goal is to compare perceptual decision boundaries across observers and models. Our work addresses this gap by using generative models to construct parametric continua of ambiguous imagery and measuring psychometric responses from both human observers and pretrained classifiers.

5. Details on Framework and Outputs

5.1. Stimuli Generation Details

Using our synthesis method, we generated 300 ambiguous stimuli for the duck-rabbit experiment (5α levels \times 6 guidance scales \times 10 seeds). In Fig. 3, we present all 300 duck-rabbit stimuli used in the duck-rabbit experiment. In addition to the duck-rabbit condition, we ran a condition of a second animal pair, creating ambiguous images between the prompts “an elephant” and “a rabbit”. In Fig. 9, we present all 300 elephant-rabbit stimuli used in the elephant-rabbit condition.

5.2. Participants

We recruited 40 participants from the local university population (undergraduate students to faculty). Twenty completed the rabbit-duck condition (16 male, 4 female; ages 21–52) and 20 completed the rabbit-elephant condition (8 male, 12 female; ages 22–36). In contrast to other perceptual and cognitive experiments, psychophysical experiments use on small number of participants over a larger number of trials in an effort to capture the internal biases and sensitivity patterns within rather than across individual observers.

All participants provided online informed consent in accordance with the Declaration of Helsinki. All procedures were approved by an Institutional Review Board. Participants used their own devices to complete the experiment, including mobile devices. One participant’s data from the duck-rabbit condition was excluded due to unrealistic response patterns, leaving $n = 19$ for duck-rabbit. Trials with response times below 150 ms or above 5000 ms were also excluded, affecting fewer than 3% of any single participant’s data.

5.3. 2AFC Task

For an overview of the perceptual evaluation framework and the 2AFC experimental design, see Fig. 4. Participants completed a two-alternative forced-choice (2AFC) task, viewing one image per trial for 500 ms followed by a response screen prompting them to choose between the two semantic labels (rabbit or duck) as quickly and accurately as

Observer \ GS	GS					
	2.5	5.0	7.5	10.0	12.5	15.0
Human	3.051	1.980	2.686	2.841	3.189	2.818
ConvNeXt-Base	1.553	0.822	1.194	0.827	1.602	0.829
DenseNet-121	1.228	1.637	1.232	0.825	0.827	0.829
EfficientNet-B0	1.192	1.186	1.228	0.822	1.429	0.827
MobileNetV3-L	0.784	0.820	0.822	0.825	0.827	0.829
ResNet-50	1.631	1.228	1.635	0.825	1.231	0.827
ViT-B/16	1.927	0.825	0.829	0.825	1.194	0.829
AlexNet	2.471	1.631	1.228	1.834	2.182	1.739
CORnet-S	1.925	0.820	0.824	1.192	1.560	1.195

Table 3. **Deviance (goodness-of-fit) across guidance scales for human observers and machine vision models.** Lower deviance values indicate better fits of the psychometric function.

possible. The next trial began automatically upon response. Each participant completed all 300 trials in random order, using the method of constant stimuli.

5.4. Classifier Models

We evaluated our ambiguous images on 8 pretrained ImageNet Classifiers [36] spanning diverse architectures and training objectives (Table 4): ResNet-50 [13], ConvNeXt-Base [25], DenseNet-121 [18], MobileNetV3-L [17], EfficientNet-B0 [41], ViT-B/16 [5], AlexNet [22] and CORnet-S [23].

We chose a variety of ImageNet-1K classifier models with varying architectures, complexities, and training schemes, evaluating their performance on our duck-rabbit and duck-elephant classification tasks. We report the various model details in Table 4. To evaluate animal responses (duck/rabbit, elephant/rabbit) in models, we assigned the relevant ImageNet-1K labels to the associated animal category, taking the mean response over the relevant labels as the response probability for the animal category (Table 5).

5.5. Psychometric Analysis

Fig. 5 shows the psychometric functions and their corresponding goodness-of-fit scores in Table 3. Goodness of fit was evaluated using the deviance statistics from psignifit, which computes the log-likelihood ratio between the fitted model and a saturated zero-residual model [43]. All deviance scores fell below the critical chi-square value $\chi^2(5, 0.95) = 11.07$, indicating acceptable fits throughout.

5.6. Bias and Sensitivity

For duck-rabbit stimuli, to visualize the effect of guidance scale and model on bias and sensitivity, we present our data from Tables 1 and 2 as bar graphs (Supplemental Figures 7 and 8). Additionally, we summarize these data with line plots in Supplemental Fig. 6.

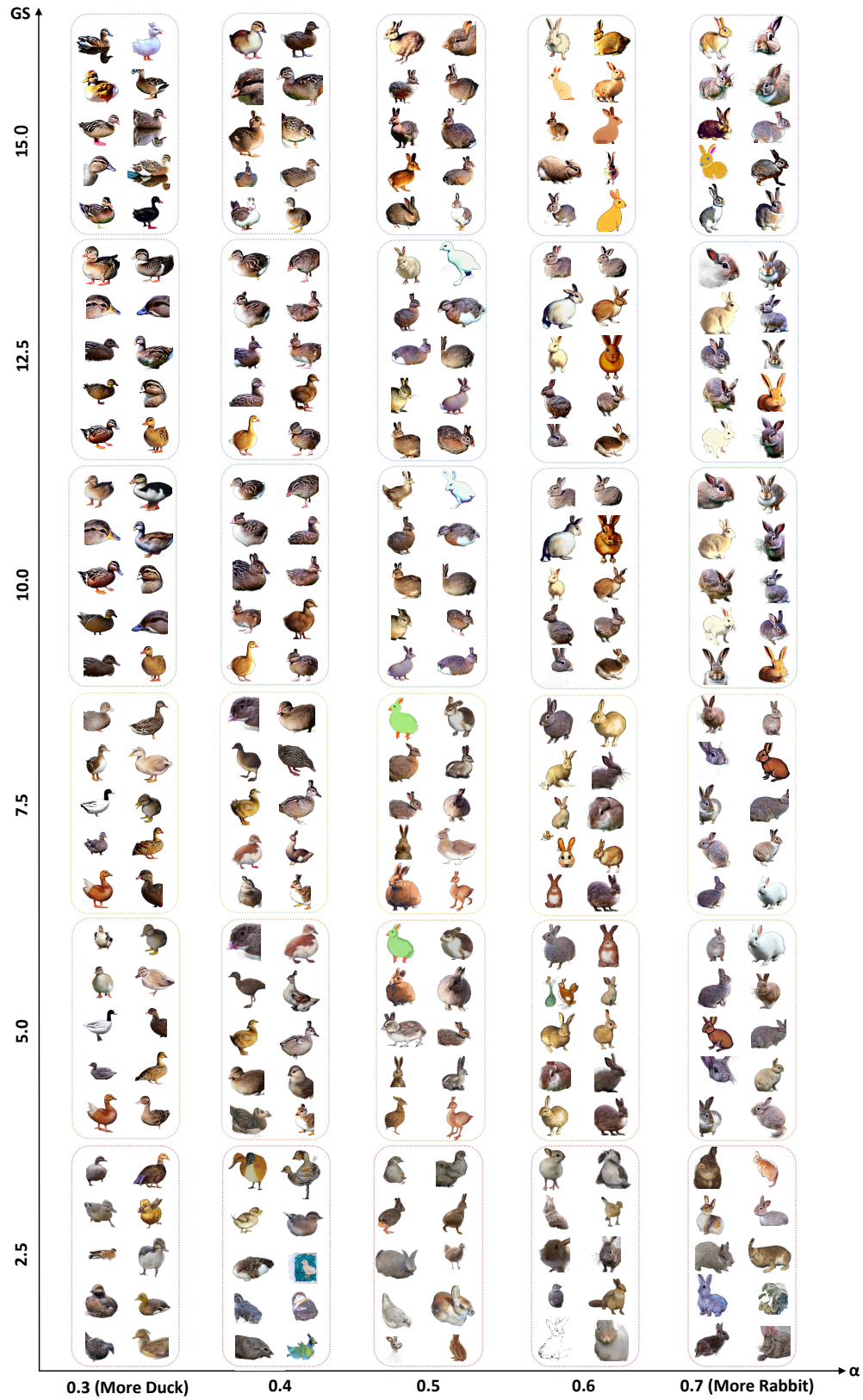


Figure 3. The 300 duck-rabbit stimuli used in the experiment, as a function of semantic mixing ratio (α) and guidance scale (GS).

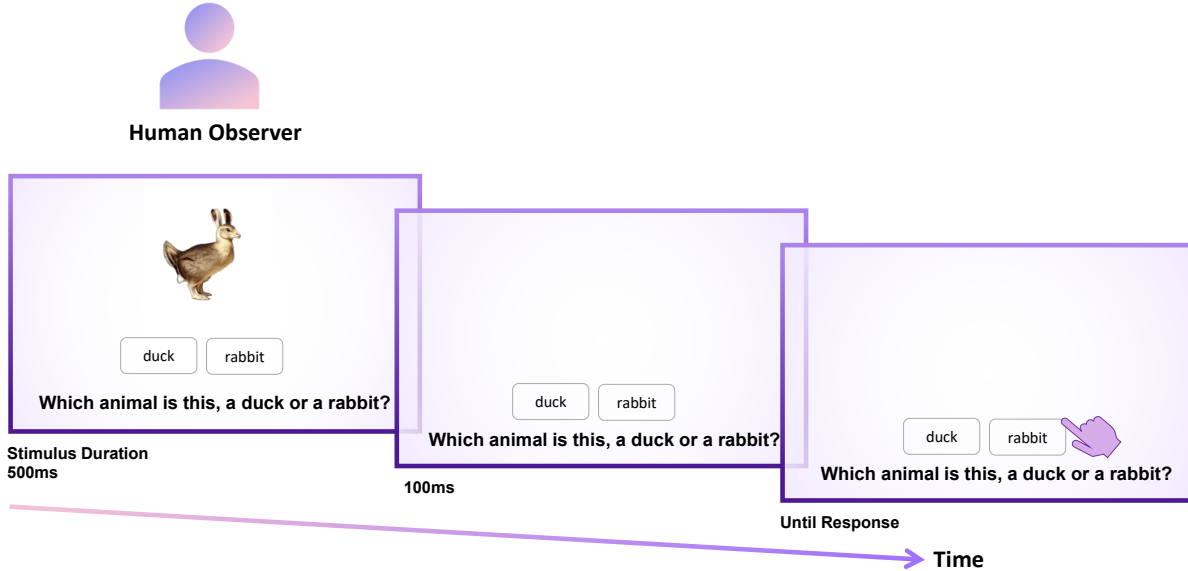


Figure 4. **Perceptual evaluation framework and 2AFC experimental design.** Participants performed a categorical two-alternative forced-choice task using ambiguous duck–rabbit images (300 trials per participant).

Category	Model	Architecture	Training Objective	Decision Space
Supervised learning (ImageNet classification)	ResNet-50 [13]	CNN	ImageNet-1K classification	1000-way softmax
	ConvNeXt-Base [25]	CNN	ImageNet-1K classification	1000-way softmax
	DenseNet-121 [18]	CNN	ImageNet-1K classification	1000-way softmax
	MobileNetV3-L [17]	CNN	ImageNet-1K classification	1000-way softmax
	EfficientNet-B0 [41]	CNN	ImageNet-1K classification	1000-way softmax
	ViT-B/16 [5]	Vision Transformer	ImageNet-1K classification	1000-way softmax
	AlexNet [22]	CNN	ImageNet-1K classification	1000-way softmax
	CORnet-S [23]	CNN	ImageNet-1K classification	1000-way softmax

Table 4. **Models used for machine psychometric evaluation.** Eight classifiers are supervised models trained for ImageNet object recognition, and evaluated with a 1000-way softmax in the duck-rabbit categories.

6. Elephant-Rabbit Condition

We apply a parallel pipeline to our duck-rabbit condition on a second ambiguous animal pairing: elephants and rabbits. This second pair serves two purposes. First, it tests whether the observed human–model differences generalize beyond a canonical bistable-inspired example. Second, it introduces a pairing with greater visual and semantic dissimilarity (e.g., large vs. small, trunk vs. ears), allowing us to probe whether bias and sensitivity depend on the structure of the underlying categories rather than the specific illusion.

In formats analogous to the duck-rabbit condition, we show the 300 elephant-rabbit stimuli (Fig. 9), tabular summaries of bias (Table 6) and sensitivity (Table 7), line plots of both bias and sensitivity trends as a function of guidance scale (Fig. 10), and bar charts of bias (Fig. 11) and sensitivity (Fig. 12).

Qualitatively, we observe similar patterns to the duck-

rabbit condition: humans exhibit lower bias than classifiers, and classifiers exhibit higher sensitivity. However, overall classifier bias is reduced in the elephant-rabbit condition, and the effect of guidance scale is less pronounced. This suggests that the magnitude of classifier bias depends on the specific label pairing, potentially reflecting differences in class priors, feature separability, or asymmetries in the learned representation space. The different machine classifier behavior further suggests that some label pairs may be less sensitive to guidance scale, possibly due to more distinct visual features. Overall, the elephant-rabbit results support the generality of our framework while highlighting that perceptual bias and sensitivity are not fixed properties of a model, but depend on the specific semantic ambiguity being probed.

Category	ImageNet-1K ID	Class Name
Duck (“a duck”)	97	drake
	98	red-breasted merganser, <i>Mergus serrator</i>
Rabbit (“a rabbit”)	330	wood rabbit, cottontail, cottontail rabbit
	331	hare
	332	Angora, Angora rabbit
Elephant (“an elephant”)	385	African elephant (<i>Loxodonta africana</i>)
	386	Indian elephant (<i>Elephas maximus</i>)

Table 5. Selected ImageNet-1k classes used for the rabbit, duck, and elephant.

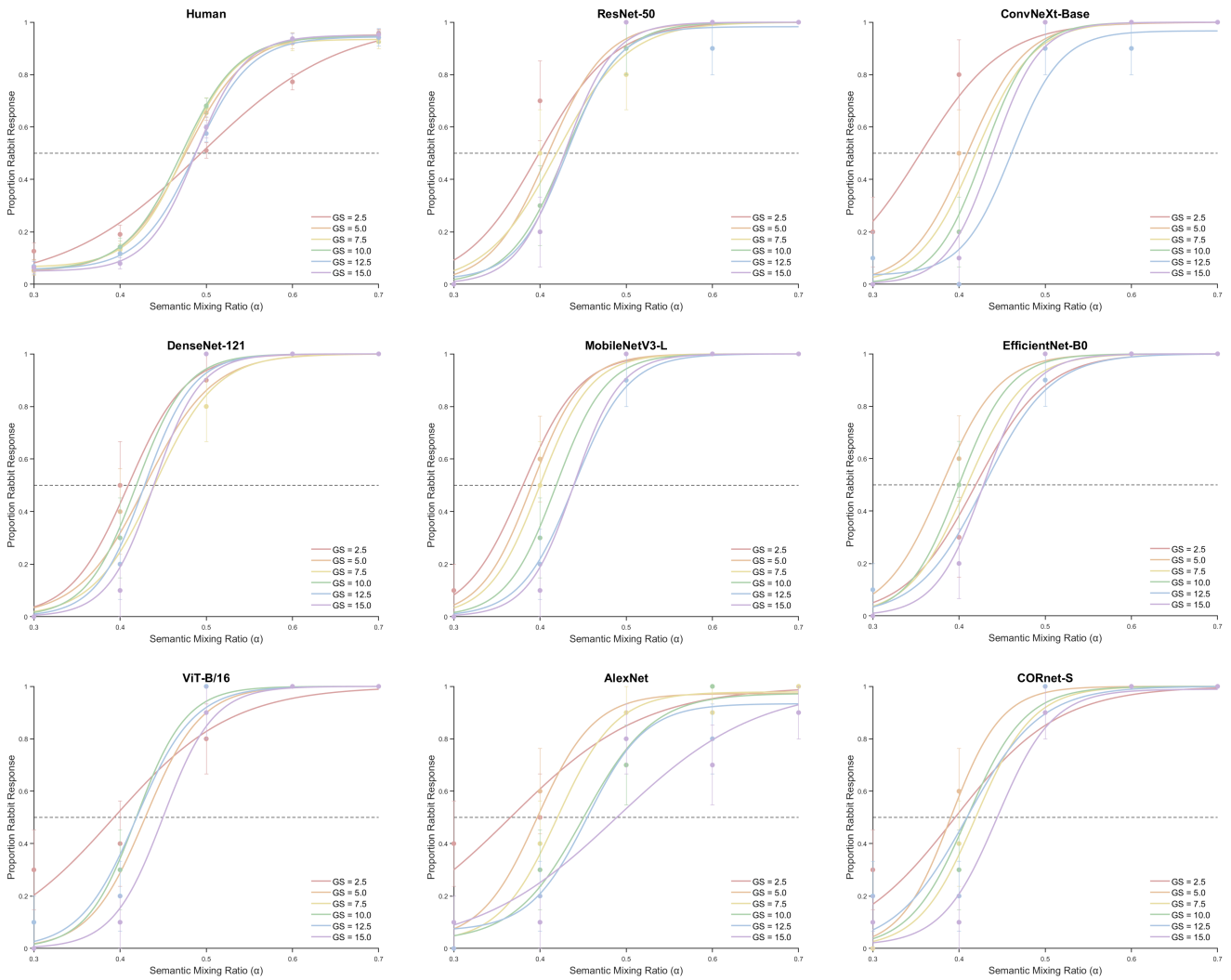


Figure 5. Psychometric functions across guidance scales for humans and machine vision models in the duck-rabbit condition. Error bars represent the standard error of the mean.

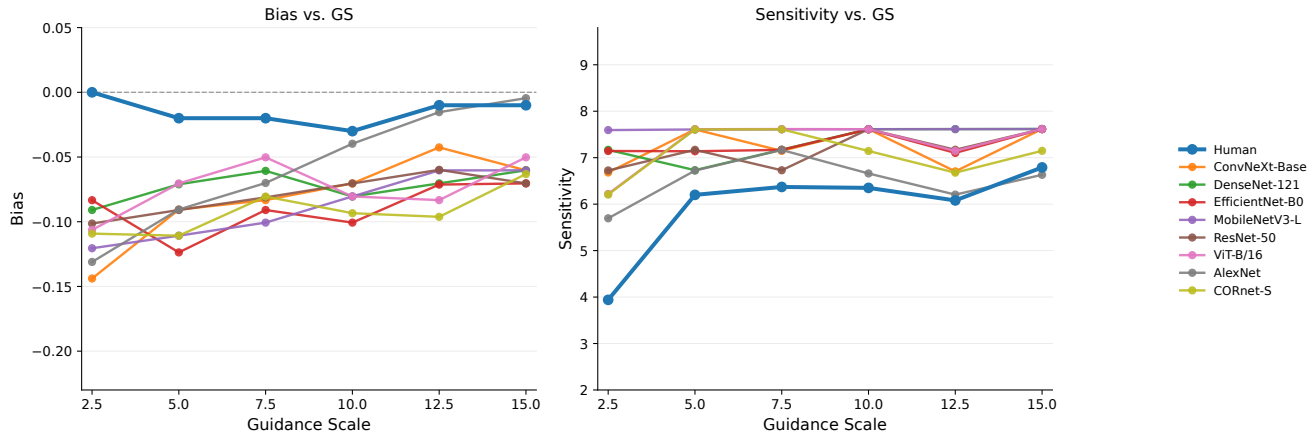


Figure 6. **Summary estimates of bias and sensitivity for duck-rabbit condition.** **Left:** Bias, computed as $PSE - 0.5$, reflects shifts in the semantic meaning boundary. The dashed horizontal line at zero indicates no bias; positive values indicate bias toward duck, values near zero indicate no bias, and negative values indicate bias toward rabbit. **Right:** Sensitivity, measured as the slope of the psychometric function at the PSE, indicates how sharply responses transition between semantic meanings.

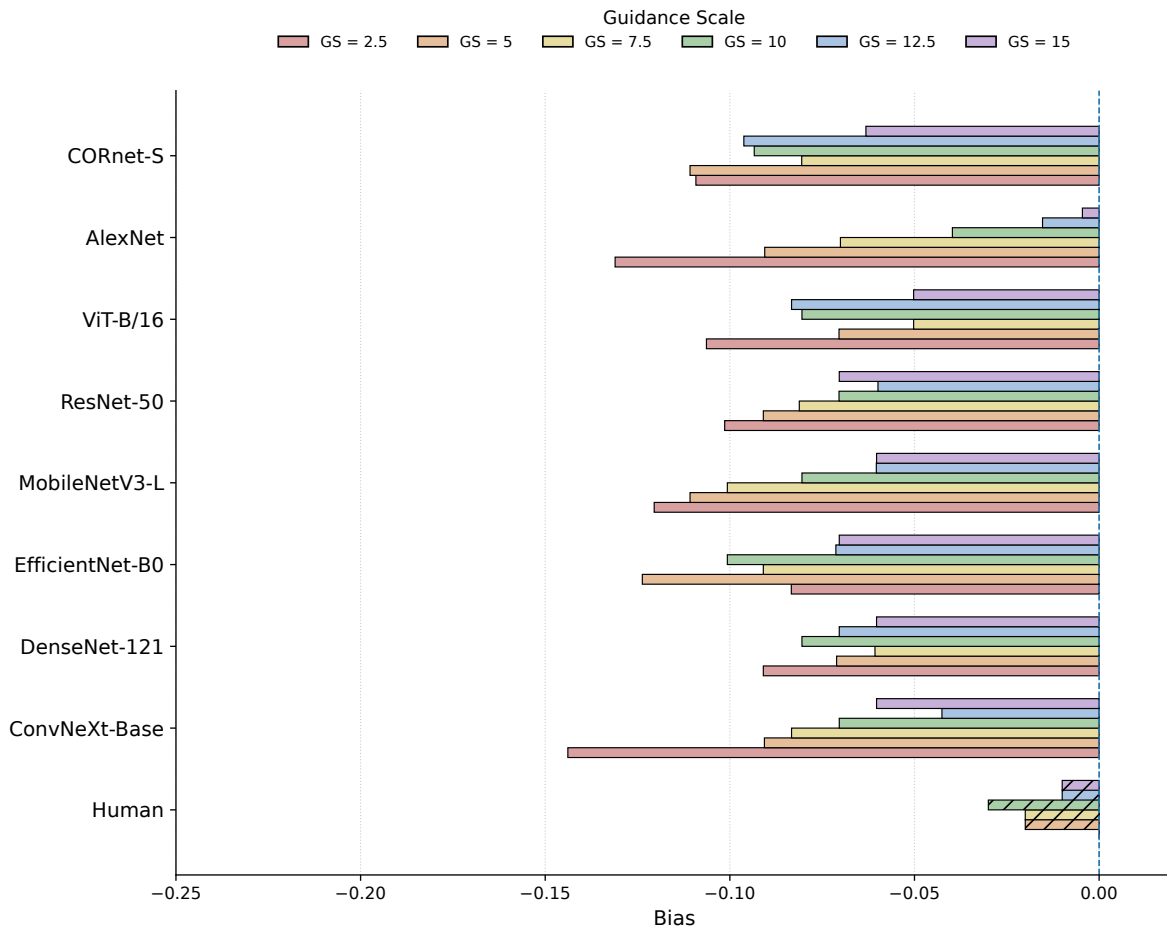


Figure 7. **Bias for the duck-rabbit condition across guidance scales for humans and classifier models.** Grouped bars show bias values computed as $PSE - 0.5$ for each model, with colors indicating different guidance scales (GS). All observers showed a negative bias, indicating they were more likely to see a rabbit than a duck even at a semantic mixing ratio $\alpha = 0.5$.

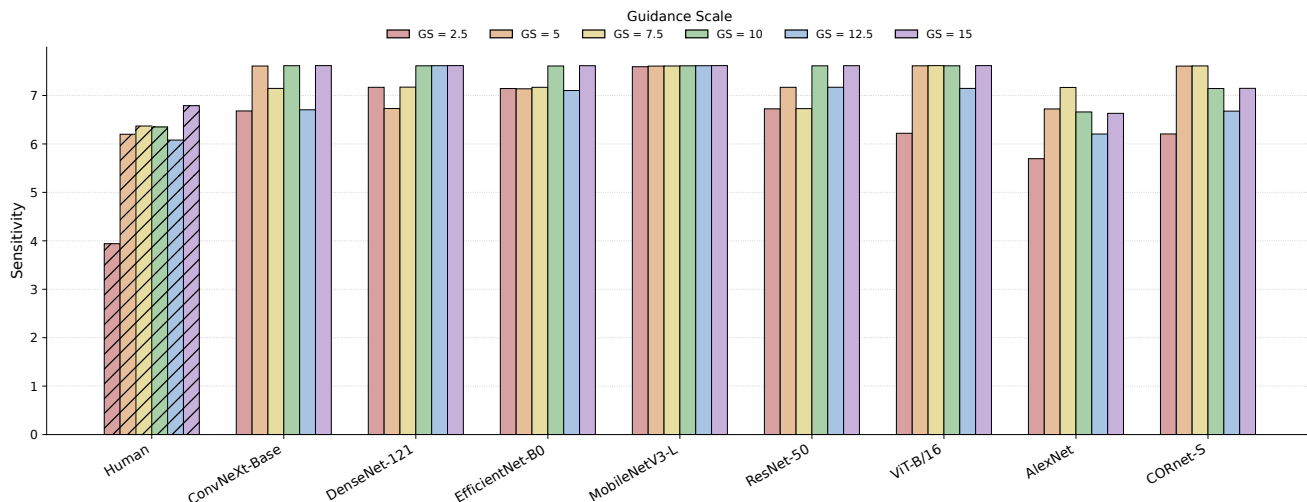


Figure 8. **Sensitivity for the duck-rabbit condition across guidance scales for humans and classifier models.** Sensitivity is quantified as the slope of the fitted psychometric function at the PSE (β_1). Grouped bars show β_1 for each model, with colors indicating guidance scales (GS). Higher sensitivity values indicate stronger semantic separation as the mixing parameter α varies. Sensitivity generally increases with guidance scale for both humans and models, although the magnitude and stability of this increase vary across architectures.

Observer \ GS	Human	ConvNeXt-Base	DenseNet-121	EfficientNet-B0	MobileNetV3-L	ResNet-50	ViT-B/16	AlexNet	CORnet-S
2.5	0.03	-0.02	0.02	0.03	-0.02	0.01	-0.02	0.04	0.02
5.0	-0.01	-0.04	-0.03	-0.06	-0.04	-0.01	-0.04	0.01	-0.04
7.5	0.00	-0.05	-0.02	-0.02	-0.02	-0.01	-0.03	0.02	-0.01
10.0	-0.01	-0.04	-0.02	-0.02	-0.02	-0.03	-0.03	0.04	-0.03
12.5	-0.03	-0.04	-0.03	-0.03	-0.04	-0.02	-0.06	0.05	-0.04
15.0	0.01	-0.03	0.00	-0.02	-0.01	-0.03	-0.02	0.00	-0.05

Table 6. **Bias for humans and classifier models across guidance scales in the elephant-rabbit condition.** Bias is defined as PSE $- 0.5$. Color intensity is computed by global min-max normalization across all entries, with negative values mapped to red (towards rabbit), positive values mapped to blue (towards elephant), and zero mapped to white (no bias).

Observer \ GS	Human	ConvNeXt-Base	DenseNet-121	EfficientNet-B0	MobileNetV3-L	ResNet-50	ViT-B/16	AlexNet	CORnet-S
2.5	3.85	7.09	7.10	6.66	6.73	6.73	5.78	5.84	6.73
5.0	5.64	7.17	7.62	6.66	7.17	6.66	7.62	7.61	7.10
7.5	6.86	7.62	7.62	7.18	7.62	7.62	7.62	6.66	7.62
10.0	8.24	7.62	7.62	7.62	7.17	7.62	7.62	7.62	7.62
12.5	6.35	7.62	7.62	6.70	7.10	7.10	6.73	6.14	7.17
15.0	6.42	7.62	7.61	7.17	7.62	7.62	7.17	6.29	6.73

Table 7. **Sensitivity for humans and classifier models across guidance scales in the elephant-rabbit condition.** Darker red indicates higher sensitivity.



Figure 9. The 300 elephant-rabbit stimuli used in the experiment, as a function of semantic mixing ratio (α) and guidance scale (GS).

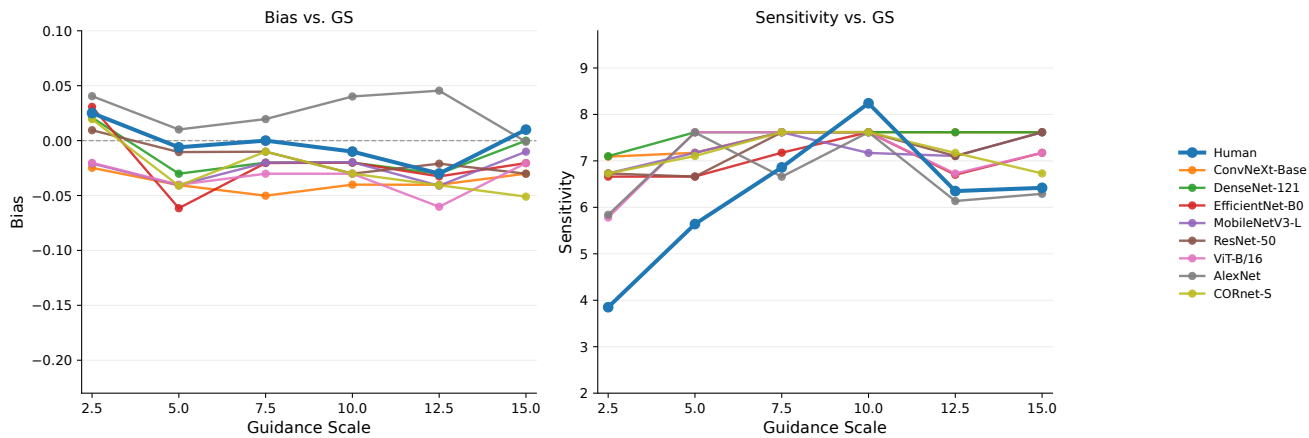


Figure 10. **Summary estimates of bias and sensitivity for the elephant-rabbit condition.** **Left:** Bias, computed as $PSE - 0.5$, reflects shifts in the semantic meaning boundary. The dashed horizontal line at zero indicates no bias; positive values indicate bias toward duck, values near zero indicate no bias, and negative values indicate bias toward rabbit. **Right:** Sensitivity, measured as the slope of the psychometric function at the PSE, indicates how sharply responses transition between semantic meanings.

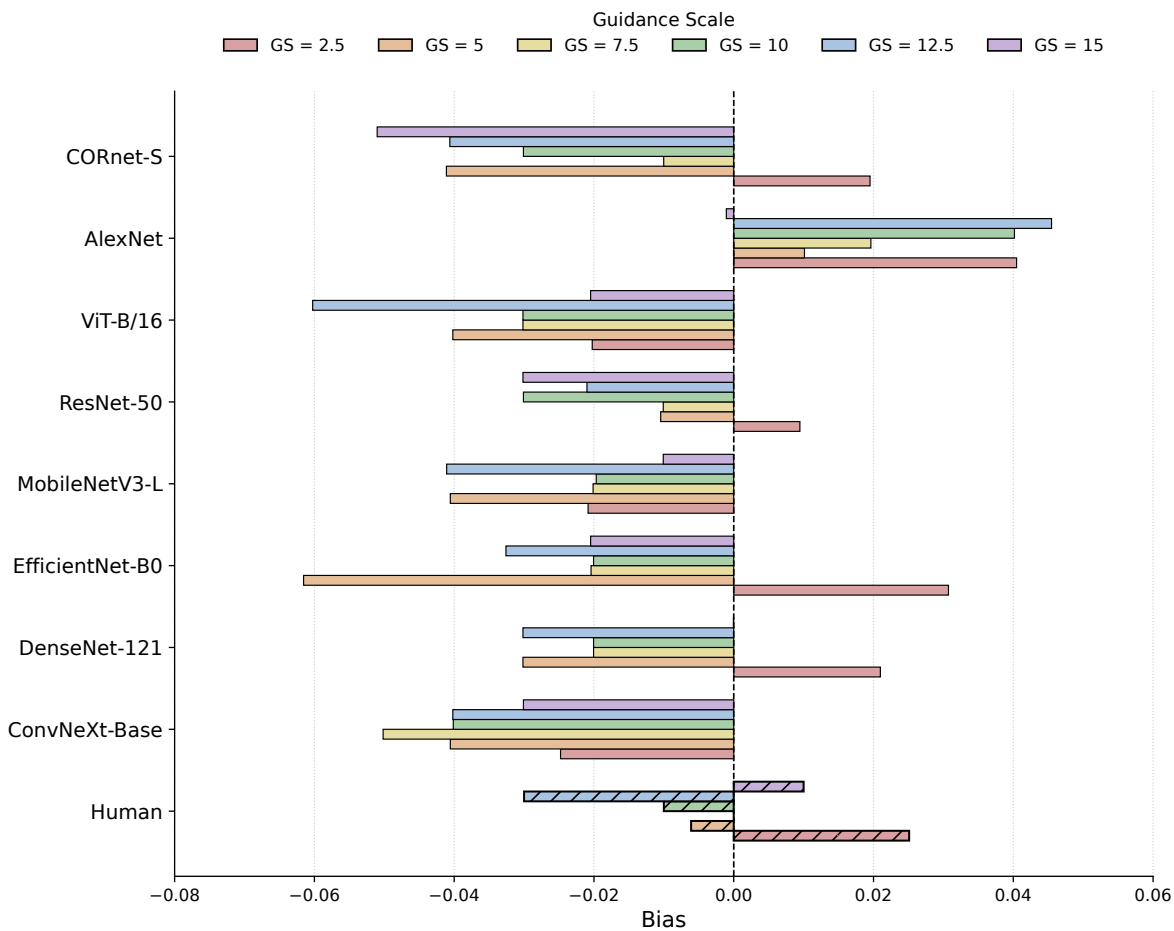


Figure 11. **Bias for the elephant-rabbit condition across guidance scales for humans and classifier models.** Grouped bars show bias values computed as $PSE - 0.5$ for each model, with colors indicating different guidance scales (GS).

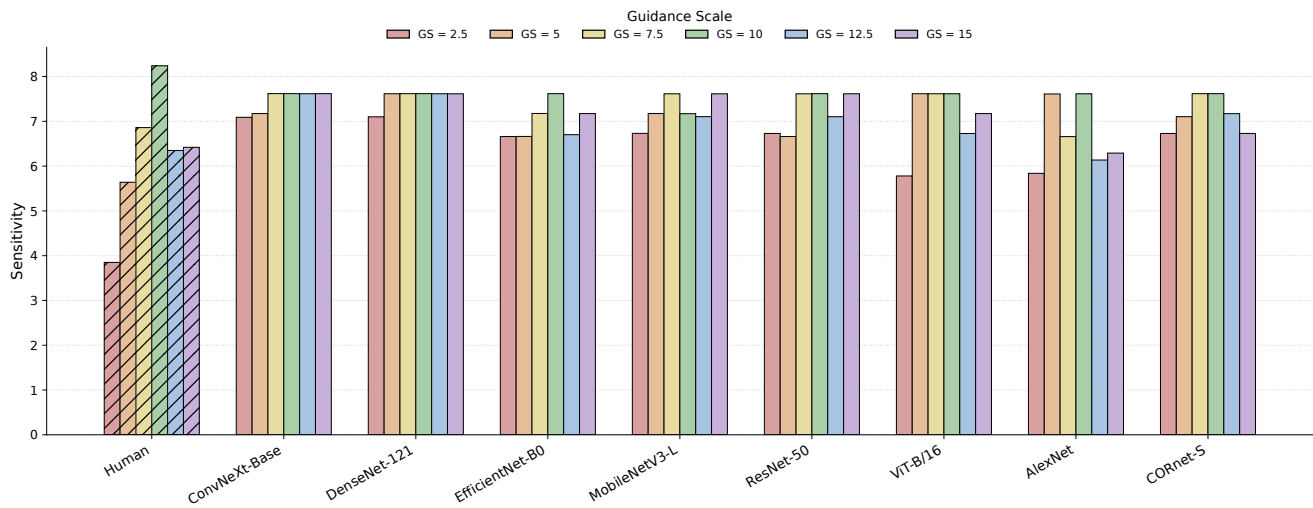


Figure 12. **Sensitivity for the elephant-rabbit condition across guidance scales for humans and classifier models.** Sensitivity is quantified as the slope of the fitted psychometric function at the PSE (β_1). Grouped bars show β_1 for each model, with colors indicating guidance scales (GS). Higher sensitivity values indicate stronger semantic separation as the mixing parameter α varies.